The Transition from Supercooled Liquid Water to Ice Crystals in Mixed-phase Clouds based on Airborne In-situ Observations

Flor Vanessa Maciel[1], Minghui Diao[1]

[1]Department of Meteorology and Climate Science, San Jose State University, San Jose, 95192, USA

5   *Correspondence to*: Minghui Diao (minghui.diao@sjsu.edu)

Abstract. The on-set of ice nucleation in mixed-phase clouds determines cloud lifetime and their microphysical properties. In this work, we develop a novel method that differentiates the early and later transition phases of mixed-phase clouds, i.e., ice crystals are initially surrounded by supercooled liquid water droplets, then as they grow, pure ice segments are formed. Using this method, we examine the relationship between the macrophysical and microphysical properties of mixed-phase clouds. The

10   results show that evolution of cloud macrophysical properties, represented by the increasing spatial ratio of regions containing ice crystals relative to the total in-cloud region (defined as ice spatial ratio), is positively correlated with the evolution of microphysical properties, represented by the increasing ice water content and decreasing liquid water content. The mass partition transition from liquid to ice becomes more significant during the later transition phase (i.e., transition phase 3) when pure ice cloud regions (ICRs) start to appear. Occurrence frequencies of cloud thermodynamic phases show significant

15   transition from liquid to ice at a similar temperature (i.e., -17.5°C) among three types of definitions of mixed-phase clouds based on ice mass fraction, ice number fraction, or ice spatial ratio. Aerosol indirect effects are quantified for different transition phases using number concentrations of aerosols greater than 100 nm or 500 nm ($N_{>100}$ and $N_{>500}$, respectively). $N_{>500}$ shows stronger positive correlations with ice spatial ratios compared with $N_{>100}$. This result indicates that larger aerosols potentially contain ice nucleating particles, which facilitate the formation of ice crystals in mixed-phase clouds. The impact of

20   $N_{>500}$ is also more significant on the earlier transition phase when ice crystals just start to appear compared with the later transition phase. The thermodynamic and dynamic conditions are quantified for each transition phase. The results show in-cloud turbulence as a main mechanism for both the initiation of ice nucleation and the maintenance of supercooled liquid water, while updrafts are important for the latter but not the former. Overall, these results illustrate the varying effects of aerosols, thermodynamics, and dynamics throughout cloud evolution based on this new method that categorizes cloud

25   transition phases.

1 Introduction

Clouds with different thermodynamic phases can have contrasting influences on the net radiation at the top of atmosphere, depending on their microphysical properties, spatial extent and the distributions of hydrometeors (Matus and L'Ecuyer, 2017). Among three types of cloud phases (i.e., ice, liquid and mixed), mixed-phase clouds contain both supercooled liquid water and

30   ice crystals. Radiative forcing of mixed-phase clouds over the Southern Ocean has large impacts on Earth's climate based on global climate model simulations (e.g., Tan et al., 2016; Hyder et al., 2018). Evaluating and improving the model parameterizations of mixed-phase clouds requires an improved understanding of their macrophysical and microphysical properties, as well as the factors controlling their formation and evolution.

Previous observations of mixed-phase clouds in the high latitudes have identified complex structure both vertically and
35   horizontally. Using aircraft-based observations over the Southern Ocean, a high frequency of supercooled liquid water was found within low-level clouds in this region, and mixed-phase cloud segments were found to be more spatially heterogeneous compared with the pure liquid and pure ice segments (D'Alessandro et al., 2021). When calculating cloud top phase frequencies as a function of cloud top temperature by using aircraft-based lidar and radar observations over the Southern Ocean, liquid phase was seen as the dominant phase for 74.9% of the cloud top cases with subfreezing temperatures, and supercooled liquid
40   water was found in cloud tops at temperatures as low as -30°C (Zaremba et al., 2020). Using a large dataset collected by the Convair 580 aircraft of the National Research Council (NRC) of Canada it was found that several microphysical properties are dependent upon temperature, including supercooled liquid droplet concentration (Nliq), ice and liquid water content (IWC and LWC, respectively) (Korolev et al., 2003).

Ice nucleation within mixed-phase clouds and the factors behind the sustainability of mixed-phase clouds are still topics of
45   contention within the field. The resilience of mixed-phase cloud system have been shown to be affected by local processes such as the formation and growth of cloud droplets and ice crystals (Morrison et al., 2012). The thermodynamics and dynamics of the atmosphere also play a large role in affecting the formation and development of mixed-phase clouds. Using observations of vertical motion within Arctic mixed-phase stratiform, Shupe et al. (2008) showed that an in-cloud updraft sustains the clouds, which also supports growth of ice and liquid mass concentrations. Their results also suggest that ice crystal
50   concentrations (Nice) are often limited in order to support the persistent supercooled liquid water. The connection between ice formation and vertical air velocity at cloud base was examined for mixed-phase clouds with less than 380-m depth by using ground-based Doppler lidar and cloud radar, and the mass flux of IWC was found to increase by two orders of magnitude when the vertical velocity fluctuation increases (Bühl et al., 2019). A study analyzed generating cells of ice crystals inside mixed-phase cloud layers over the Southern Ocean and found that these generating cells have small horizontal widths and contain
55   supercooled liquid water with higher LWC and Nliq than that of the areas between the generating cells, which also held true for ice particles whose dispersions, number concentration, and sizes are larger within the generating cells (Wang et al., 2020). With seven years of ground-based observations an Alaskan site, it was found that Arctic mixed-phase clouds occur less often in the early fall when the winds are southerly as the atmosphere is more stable, drier, colder and has lower relative humidity. Conversely, during northerly winds they have a wider particle distributions (Qiu et al., 2018).

60   Aerosols have been documented to influence the microphysical properties of mixed-phase clouds around the globe. Field study observations over a fourteen-year time period and from various locations around the Earth were combined to show that both temperature and the number concentration of aerosols larger than 0.5 μm in diameter can impact the concentrations of growing ice nuclei in mixed-phase clouds (DeMott et al., 2010). From aircraft observations over the Arctic, it was found that

entrainment above mixed-phase clouds could enhance Nice and aerosol thermodynamic indirect effect likely occur (Jackson

65 et al., 2012). Using a nine-year long aerosol dataset, Norgren et al. (2018) found that clean mixed-phase clouds with lower aerosols loading have a higher IWC at their base compared with clouds with a higher aerosol loading. Other studies over the Southern Ocean, e.g., McFarquhar et al. (2021), showed that those environments are primarily pristine, suggesting limited long-range continental aerosol transport and potentially more aerosols newly formed over the high southern latitudes. Observations and simulations of ice nucleating particles (INPs) showed that sea spray aerosol may play a major role to initiate

70 primary ice nucleation in low-level mixed-phase clouds over the Southern Ocean (McCluskey et al., 2019). Besides primary ice production, secondary ice production has also been shown to be a critical process enhancing Nice in mixed-phase clouds based on both in-situ airborne observations (Huang et al., 2017; Järvinen et al., 2022) and global climate simulations (Zhao and Liu, 2021) over the Southern Ocean. Secondary ice production can also be affected by aerosol loading, e.g., higher concentrations of cloud condensation nuclei can lead to higher supercooled liquid droplet concentrations, and therefore

75 reducing the efficiency of rime-splintering process.

These aforementioned studies demonstrated that the coexistence and interaction between supercooled liquid droplets and ice crystals hold a key for understanding the persistence of mixed-phase clouds despite of ice–liquid mixtures being unstable. An examination of aerosol indirect effects on liquid and ice hydrometeors separately is a also critical step towards a better understanding of the net aerosol indirect effects on the entire cloud (Korolev et al., 2017; Storelvmo, 2017). Targeting these

80 topics, in this work, we develop a method to identify several transition phases of mixed-phase clouds, by using the spatial relationships between segments containing only ice, only liquid, or both ice and liquid. In section 2, a description of the observation dataset and instruments is given. In section 3, the details of the identification of four transition phases, their occurrence frequencies, and comparisons with previously established mixed-phase cloud definitions are provided. In addition, the relationships between macrophysical and microphysical properties of mixed-phase clouds during their evolution are

85 examined. Aerosol indirect effects from larger and smaller aerosols are quantified, followed by a contrast of thermodynamic and dynamic conditions among these transition phases. Lastly, in section 4, we discuss the applications of this method for contrasting different definitions of mixed-phase clouds, and the implications of model parameterizations.

2 Observational Dataset

2.1 SOCRATES In-situ Observations and Instrumentation

90 The U.S. National Science Foundation (NSF) Southern Ocean Clouds, Radiation, Aerosol Transport Experimental Study (SOCRATES) flight campaign was conducted from January 15th to February 24th in 2018 (McFarquhar et al., 2021). This NSF-funded campaign utilized the NSF/National Center for Atmospheric Research (NCAR) Gulfstream V (G-V) research aircraft which flew over the Southern Ocean region of 62°S-42°S and 133°E-164°E as shown in Figure 1. A total of fifteen research flights (RFs) in this campaign were performed with a combined total of 111 flight hours flown. In this work, we applied a

temperature restriction of −40°C to 0°C, commonly known as the mixed-phase cloud regime as this temperature range allows for the occurrence of both ice particles and supercooled liquid water, for all our analyses.

The NSF G-V research aircraft during the SOCRATES campaign was equipped with various scientific instruments to measure the various characteristics of the atmosphere, such as aerosol number concentrations (Na), cloud microphysical properties and common meteorological components – temperature, pressure, wind speed and humidity. The temperature was measured by the Rosemount temperature probe. To measure the water vapor molecule number density at 25-Hz resolution the Vertical Cavity Surface Emitting Laser (VCSEL) hygrometer was used. The final data reported the water vapor mixing ratio in 1-Hz resolution and a corrected version of water vapor data based on a post-campaign calibration in summer 2018 is used in this study (Diao, 2021). The water vapor and temperature data are used to calculate relative humidity with respect to liquid and ice (RH_{liq} and RH_i), by using the equations for saturation vapor pressure with respect to liquid and ice from Murphy and Koop (2005), respectively. The uncertainties associated with RH_{liq} and RH_i originate from both water vapor and temperature measurements, which sum up to 6%–7% for the mixed-phase cloud regime. We placed a ceiling on RH values by restricting all RH_{liq} greater than 101% to 101%. The hydrometeor measurements used in this study were obtained from the Two-Dimensional Stereo Probe (2DS) and the cloud droplet probe (CDP), which have size ranges at $40 – 5000$ μm and $2 – 50$ μm, respectively. Aerosols number concentration and size distribution are measured by the Ultra-High Sensitivity Aerosol Spectrometer (UHSAS) which has a size range of $60 – 1000$ nanometers (nm).

2.2 Two Previous Datasets for Cloud and Hydrometeor Thermodynamic Phase Classifications

For this work, two previously published datasets regarding thermodynamic phase classifications for the SOCRATES observations are used. Both datasets cover all research flights in SOCRATES campaign with the exception of research flight 15 due to the malfunction of 2DS probe. The first dataset reports cloud phase (ice, liquid or mixed) at 1-Hz resolution, which was mainly derived from the 2DS and CDP cloud probes (Yang et al., 2021). That method was also verified by other cloud probes, such as the King probe for detecting liquid water content, and the Rosemount Icing Detector for detecting the existence of supercooled liquid water by freezing them when they collide with the detector and changing its constant vibration frequency. The second dataset for detecting individual hydrometeor's thermodynamic phase (either ice or liquid) is also used, which was produced by the University of Washington with the Ice-Liquid Discriminator (UWILD) through a machine learning approach (Atlas et al., 2021; Mohrmann, et al. 2021). Each particle imaged by the 2DS probe is classified particle-by-particle into ice, liquid or unclassified, as 0, 1 and NaN, respectively. In this dataset, the group also provides 1-Hz aggregated data for each research flight that include a quantification of phase separated particle size distributions. We use the hydrometeor count defined by the maximum diameter in the UWILD dataset to calculate the ice particle number fraction, which is dividing the number of ice particles by the total number of ice particles plus liquid droplets in one second.

3 Results

3.1 A Method of Mixed-Phase Cloud Transition Phase Classification

A classification method of the transition phases of mixed-phase clouds is developed for 1-Hz aircraft-based observations,
which mainly involves two steps. In the first step, three types of cloud segments are identified for each second of observations,
130   including liquid cloud region (LCR), ice cloud region (ICR), and mixed-phase cloud region (MCR). LCR is defined as a second
of in-cloud segment where only supercooled liquid droplets were observed, while ICR is defined as a segment with only ice
crystals. MCR is the segment with occurrence of both ice and liquid. Here the identification of liquid and ice at 1-Hz resolution
is based on the 1-Hz cloud thermodynamic phase data published in Yang et al. (2021). In the second step, a total cloud region
(TCR) that can potentially contain a combination of LCR, ICR and MCR is identified, which basically is a consecutive in-
135   cloud segments. For instance, if five seconds of LCR are adjacent to one second of MCR, then both the LCR and MCR belong
to the same TCR. Within each TCR, the spatial ratio of LCR, MCR, and ICR relative to TCR is defined as M1, M2 and M3,
respectively. Following the calculation of these spatial ratios, four transition phases are defined as follows: (1) only ICR
appears in the TCR, (2) MCR coexists with LCR, but no ICR exists, (3) ICR appears and it either resides with LCR, MCR, or
both, (4) only ICR appears in the TCR. In other words, phases 1 and 4 stand for pure liquid and ice cloud segments, respectively.
140   Phase 2 represents the first appearance of ice crystals as they are embedded in MCR and surrounded by supercooled liquid
droplets. Phase 3 represents the evolution from MCR to ICR, as pockets of pure ice segments start to appear.

The four transition phases are depicted in an idealized diagram in Figure 2. The calculation of spatial ratios and the definition
of each transition phase are summarized in Table 1. A potential evolution pathway from phase 1 to 4 is depicted in this idealized
diagram, but we caution that a mixed-phase cloud may or may not follow this exact pathway in the real atmosphere, as certain
145   transition phase may be skipped, the evolution direction could be reversed, and multiple phases can appear in the same cloud
in a 3-D view. Nevertheless, this method provides a statistical separation of the cloud transition phases and allows a more
focused analysis of the coexistence of supercooled liquid water and ice crystals that cannot be achieved solely based on second-
by-second measurements (i.e., if one only analyzes seconds with coexisting ice and liquid).

Figure 3 shows the number of 1-second samples for each transition phase as well as their probability among all transition
150   phases within 5-degree temperature bins. The results show that phases 1 and 5 are more dominant at higher and lower
temperatures, respectively, which follows the basic thermodynamic process that the transition from liquid to ice phase occurs
more frequently at lower temperatures. At temperatures between -20°C and -5°C, phase 3 is the most dominant phase and
contributes to 80% to 40% of the total samples, while phase 2 contributes to 20% - 40% of the total samples. The fact that the
pure ice or liquid phase only contribute to 10% - 20% of the total samples between -20°C and -5°C demonstrates that the cloud
155   segments sampled in the SOCRATES campaign are spatially heterogeneous, consistent with the results in the previous study
of D'Alessandro et al. (2020).

3.2 Occurrence Frequencies of Cloud Phases Compared Among Various Phase Identification Methods

The distributions of three cloud thermodynamic phases (ice, liquid and mixed) are compared between three types of phase identifications, including (i) the 1-Hz cloud phase distribution defined by Yang et al. (2021) using the ice mass fraction (i.e.,
160   IWC/TWC) derived for 1-second observations, i.e., liquid, mixed and ice phases defined as ice mass fraction < 0.1, $0.1 - 0.9$ and > 0.9, respectively; (ii) cloud phase distribution defined by the majority of the hydrometeors by particle count using the UWILD data, i.e., liquid (ice) phase defined as a second of data with more than 90% (less than 10%) of hydrometeor particle count being liquid droplets, and mixed phase defined as a second of data with 10% - 90% of particle count being liquid droplets; (iii) cloud phases defined by the ice spatial ratio within each TCR using the method developed in this work. That is, for each
165   TCR, ice spatial ratio is calculated as length of (ICR+MCR) / length of TCR. Liquid, mixed, and ice phases are defined as where ice spatial ratio of an entire TCR is < 0.1, $0.1 - 0.9$ and > 0.9, respectively. To summarize, each of these three types of method relies on a certain type of fraction of ice crystals relative to the total hydrometeors, either in terms of 1-Hz mass fraction, 1-Hz particle number fraction, or in terms of the spatial fraction relative to the entire cloud segment.

Figure 4 shows the occurrence frequencies of cloud thermodynamic phases in relation to temperature compared among three
170   identification methods. The results show that the ice spatial ratio (Figure 4 a) and ice mass fraction (Figure 4 c) methods have similar distributions of three thermodynamic phases. The ice spatial ratio method has slightly higher mixed phase frequency than the ice mass fraction method. For the ice particle number fraction method (Figure 4 b), the mixed phase frequency is the highest among all three methods, at $0.1 - 0.2$. At temperatures above -20°C, ice crystals often have larger size dimension but smaller number concentration than supercooled liquid droplets, meaning that when ice number fraction is less than 0.1 (liquid
175   phase in Figure 4 b), ice mass fraction may exceed 0.1 and becomes mixed phase in Figure 4 c. For the lowest temperature bin close to -40°C, the particle-by-particle identification may have difficulties discerning single hydrometeors as frozen droplets, supercooled liquid droplets or small ice crystals, which leads to the large increase in mixed phase frequency in that bin. Overall, all three methods show a significant transition from liquid to ice phase at a similar temperature around -17.5°C. This indicates that the major transition from liquid to ice are reflected in both cloud microphysical (i.e., mass partition and number partition)
180   and macrophysical properties (spatial extent partition).

3.3 Relationship between Microphysical and Macrophysical Properties of Mixed-phase Clouds

The cloud particle size distribution (PSD) for four transition phases is shown in Figure 5, separately plotted for the 2DS and CDP probes. Measurements from both probes have been identified in any of the four transition phases, since either probe can possibly measure ice or liquid. Phase 1 and 2 both have the highest concentration of small liquid droplets between $2 - 10$ µm.
185   Phase 2 has the highest concentration of hydrometeors at $10 - 60$ µm, while phase 3 has the highest concentration at $60 - 3000$ µm. Phase 4 also has relatively high concentrations of ice crystals at $200 - 3000$ µm, but they are lower than the values from phase 3 by a factor of $5 - 10$. The decreasing ice crystal concentration per size bin from phase 3 to phase 4 may be caused by stronger sedimentation of ice crystals in phase 4, or by stronger secondary ice production in phase 3. The significant decrease

(1 to 4 orders of magnitude) of hydrometeor concentration per size bin at 2 – 60 µm in phase 4 compared with other three
190   phases suggest that most supercooled liquid water may transition into ice phase through Bergeron process or riming, instead
of the freezing of individual droplets. In addition, smaller supercooled liquid droplets require lower temperatures to freeze into
ice crystals. This feature is also shown in Figure 6, as small ice crystals at 2 – 60 µm size range show increasing concentrations
with decreasing temperatures. An additional cloud probe – the Fast 2-Dimensional Cloud (Fast-2DC) probe is also examined
in Figures 5 and 6. Even though the 2DC probe had more problematic measurements compared with 2DS probe due to cloud
195   imaging issues during SOCRATES, the two probes (2DS and 2DC) still show similar PSD results for three transition phases
containing ice crystals (i.e., phases 2, 3 and 4), indicating that the differences seen among transition phases are less likely
caused by instrument uncertainties.

The relationship between cloud macrophysical properties (represented by ice spatial ratio) and several microphysical properties
are further examined, including ice particle number fraction (Figure 7), LWC, IWC and ice mass fraction (Figure 8). A linear
200   regression of the ice spatial ratio against each microphysical property is shown for transition phases 2 and 3, separated by
LCR, MCR and ICR. Slope value (b) of the linear regression is provided in the text legend. Since transition phase 2 does not
contain ICR, no data points are shown in those sub-panels in Figures 7 – 9.

All regions (i.e., LCR, MCR and ICR) in Figure 7 show positive correlations between ice particle number fraction and ice
spatial ratio in phases 2 and 3. This means that while ice crystals gradually dominate the total particle population (supercooled
205   liquid droplets plus ice particles) in a particular second, the segments containing ice particles (i.e., MCR+ICR) also start to
dominate the spatial extent of the entire cloud segment (TCR) from a macroscopic perspective. Comparing phase 2 and 3,
phase 2 (without ICRs) show smaller positive correlation (b values of 0.24 and 0.35) compared with phase 3 (b values of 0.67,
0.47, and 0.52). This is because when ice particles are surrounded by supercooled liquid water, the latter has much higher
number concentration than ice crystals and therefore ice particle number fraction are relatively low, ranging from 0 to 0.2 on
210   average in phase 2. On the other hand, in phase 3, ice crystals start to become the dominant particles by number concentration
when ICR appears, and supercooled liquid water becomes less dominant. Similar slope values in Figure 7 b, d and f indicate
that the rates of change of ice particle number fraction in LCR, MCR and ICR are similar. That is, as the entire segment TCR
becomes more ice dominant, individual small segments embedded inside also experience similar rate of transition from liquid
to ice based on number concentrations, except that the ICR has higher ice particle number fraction on average (i.e., higher
215   intercept values), followed by MCR, then LCR.

Previously, Wang et al. (2020) used airborne remote sensing measurements from SOCRATES campaign to identify generating
cells of ice crystals. Their study showed that inside the generating cells, larger ice particles and higher ice number concentration
were seen, associated with the updrafts inside the cells. These reported generating cells are also analyzed in Figure 7, which
shows their average values in each ice spatial ratio bin. The generating cells associated with smaller ice spatial ratio contain
220   lower ice particle number fraction. But when the generating cells are associated with higher ice spatial ratio (> 0.5),
significantly higher ice particle number fraction (around 0.6 to 1) is seen. This result suggests that not all regions within the

generating cells experience significant phase transition from liquid to ice, unless the ice-containing regions become dominate in terms of spatial extent.

Figure 8 shows the correlations of LWC and IWC with respect to ice spatial ratio. A clear negative slope is seen in Figure 8
225   a–d, indicating that as the ice spatial ratio increases, the LWC decreases. On the contrary, a positive trend is seen in Figure 8 e, f and h, indicating increasing IWC with increasing ice spatial ratio. These results are consistent with the analysis of ice particle number fraction, which show that the increasing dominance of ice crystals in both mass and number concentrations is correlated with the increasing spatial ratio of ice-containing regions. Slope values in Figure 8 illustrate that in phase 2 and 3, LWC decreases more significantly in LCR (b = -0.60) than MCR (b = -0.14). Compared with phase 2, phase 3 shows even
230   stronger decrease of LWC in LCR and MCR with b = -1.5 and -0.70, respectively. For the changes of IWC, the slope values are similar between MCR and ICR in phase 3 (b = 1.4 and 1.5, respectively), and are slightly lower for MCR in phase 2 (b = 1.14). These results indicate that IWC has similar rate of increase between ice crystals embedded among supercooled liquid droplets (i.e., MCR) and ice crystals in pure ice segments (i.e., ICR). However, the decrease of LWC becomes more significant by a factor of 3 once pure ice segments appear in phase 3 compared with phase 2.

235   Figure 8 i and j show the positive correlations between ice mass fraction and ice spatial ratio. Ice mass fraction increases more rapidly with increasing spatial ratio in phase 3 than phase 2, with slope values of 0.88 and 0.19, respectively. This result indicates that when ice crystals first appear in MCR, the mass partitioning is still dominated by liquid phase even if ice crystals appear in a high spatial fraction of the cloud segment. As ice crystals grow into pure ice segments (i.e., ICR), liquid phase starts to rapidly transition into ice phase, suggesting that the formation of pure ice segment is a key step for Bergeron process
240   to become highly effective. This result also indicates that even though ice and supercooled liquid water coexist throughout the lifetime of mixed-phase clouds, the partition between them has different rates of change during different transition phases.

3.4 Aerosol Indirect Effects on the Evolution of Mixed-phase Clouds

The relationship between aerosol number concentration and ice spatial ratio is examined in Figure 9. Number concentrations of larger aerosols (diameters > 500 nm, namely $N_{>500}$) and smaller aerosols (diameters > 100 nm, namely $N_{>100}$) are analyzed
245   in a – h and i – p, respectively. The slope values of the linear regressions show strong positive correlations between $N_{>500}$ and ice spatial ratio in phase 2, when ice crystals just start to appear and are surrounded by supercooled liquid droplets. Such positive correlation becomes weaker in phase 3, when ICR start to appear. The stronger positive correlation with $N_{>500}$ in phase 2 is likely due to primary ice nucleation (such as heterogeneous nucleation) playing a major role in phase 2 when ice crystals first start to appear. On the other hand, secondary ice production may occur more frequently in phase 3, and secondary ice
250   production via rime-splintering is less effective when concentrations of cloud condensation nuclei are higher. For the correlations with $N_{>100}$, positive trend is still seen with respect to ice spatial ratio in MCR and ICR, indicating possible heterogeneous nucleation pathway of ice formation. Negative correlations between $N_{>100}$ and ice spatial ratio in LCR suggest that without ice nucleating particles to facilitate ice formation (hence the pure liquid segment LCR), higher aerosol number

concentration may impede the growth of ice segments. Overall, the weaker positive correlations with $N_{>100}$ in MCR and LCR
compared with $N_{>500}$ indicates that larger aerosols play a more dominant role for initiating ice nucleation than smaller aerosols.

3.5 Thermodynamic and Dynamic Effects on the Evolution of Mixed-phase Clouds

Thermodynamic and dynamic conditions of each transition phase are examined at various temperatures in Figure 10, based on
distributions of RH_{liq}, RH_i, vertical velocity (w) and standard deviation of w (σ_w, calculated for every 40 seconds). In addition,
a similar analysis in relation to ice spatial ratio is shown in Figure 11. In the distribution of RH_i and RH_{liq}, phase 2 shows the
highest RH values, followed by phases 1 and 3. Phase 4 has the lowest RH_i and RH_{liq} values. Comparing RH_i values in regions
with and without ice, phase 2 shows higher RH_i for regions with ice, while phase 3 shows higher RH_i in regions without ice.
This feature can be explained by the fact that higher RH_i is required in order to initiate ice nucleation in phase 2, while ice
crystals that continue to grow in phase 3 will further reduce RH_i magnitude by vapor deposition. Based on Figure 7, IWC is
also lower in phase 2 than phase 3, which suggests that ice crystals in phase 2 would be less effective for relaxing ice
supersaturation than those in phase 3.

For distributions of w, phase 1 has slightly higher w than other phases. Phase 2 – 4 show slightly negative w values, suggesting
weak downdrafts as the predominant condition in mixed-phase clouds. For the σ_w distribution, regions with ice in phase 2 have
the highest fluctuations of vertical velocity, indicating that stronger in-cloud turbulence induces high RH_i (as shown in a),
which further initiates ice nucleation in phase 2. This result suggests that in-cloud turbulence may be a more prominent
mechanism to initiate transition from liquid to ice phase, compared with large-scale uplift (which would be reflected in mean
vertical velocity if that was the case). Such result is consistent with the finding of Bühl et al. (2019) which showed a positive
correlation between IWC mass flux and vertical velocity fluctuation, but this study further illustrates that in-cloud turbulence
is particularly important for the early transition phase when ice crystals first start to appear.

For the relationship between RH and ice spatial ratio (Figure 11 a and b), phase 2 shows nearly constant RH_{liq} close to liquid
saturation (within 5% of liquid saturation, which may be caused by combined uncertainties from water vapor and temperature
measurements), except when ice spatial ratio exceeds 0.9. Differing from phase 2, phase 3 shows decreasing RH_{liq} with
increasing ice spatial ratio, ranging from 98% to 83% RH_{liq}. These results indicate that before the appearance of ICR, ice
crystals embedded in MCRs do not relax liquid saturation to ice saturation since liquid droplets can still provide additional
water vapor by evaporation (e.g., the Bergeron process). But when ICR starts to appear, RH relaxes to around ice saturation
once ice spatial ratio exceeds 0.5. These results are consistent with the previous finding by D'Alessandro et al. (2021) that
RH_{liq} initially is close to liquid saturation with lower ice mass fraction but deviates from liquid saturation as ice mass fraction
increases.

For mean values of w (Figure 11 c), higher w is seen at lower ice spatial ratio, meaning that the segments containing more
supercooled liquid droplets are subject to more updrafts, while the segments containing more ice crystals are subject to more
downdrafts. This finding is consistent with Shupe et al. (2008) which pointed out the importance of updrafts for sustaining
mixed-phase clouds. Differing from the previous studies, our method can further specify that the highest updrafts are found in

the later transition phase when pure ice segments start to appear, consistent with the fact that RH_{liq} deviates more from liquid saturation in phase 3 (Figure 11 b), and therefore higher updrafts would be required to maintain supercooled liquid droplets.

290 Analysis of σ_w distribution (Figure 11 d) consistently shows that ice-containing regions in phase 2 have the highest vertical velocity fluctuations, especially for higher ice spatial ratios. But for other phases, vertical velocity fluctuations are higher for low ice spatial ratios. These results indicate that both the initiation of ice nucleation and the sustainability of supercooled liquid water are supported by in-cloud turbulence, while updrafts play an important role in the latter but not the former.

4 Discussion and Conclusions

Mixed-phase clouds are ubiquitous in the atmosphere and in order to fully capture their extent of impacts on Earth's climate,
295 more studies need to be conducted in order to investigate their formation, evolution, and aerosol effects on their microphysical and macrophysical characteristics. Therefore, in this study, a novel method that categorizes mixed-phase cloud evolution into four transition phases was presented. This method allows an investigation on the evolution of cloud macrophysical and microphysical properties, as well as the related aerosol indirect effects, as supercooled liquid water transitions to ice crystals. The relationships between microphysical and macrophysical properties are examined, which addresses the question of whether
300 the dominance of ice crystals in hydrometeor mass or number concentration also leads to a dominance of ice-containing regions in a consecutive in-cloud segment. A spatial extent parameter – ice spatial ratio – is used to identify the evolution from supercooled liquid water-dominant to ice-dominant mixed phase clouds. Positive correlations of ice particle number concentration and IWC in relation to ice spatial ratio are seen in both transition phases 2 and 3. Comparing phases 2 and 3, the latter phase shows higher rates of changes in all three microphysical properties with increasing ice spatial ratio, including faster
305 increase of ice number fraction, faster increase of IWC, and faster decrease of LWC. These results indicate that when ice crystals become more dominant and ICR starts to appear, both the mass and number partitions between liquid phase and ice phase experience a higher rate of transition.

The correlations between various cloud properties are further demonstrated by using three methods to define ice, liquid, and mixed phases. Following the generic definition of mixed-phase clouds described in Korolev et al. (1998) and Korolev et al.
310 (2017), $\mu_{ice} = \alpha_{ice} / (\alpha_{ice} + \alpha_{liq})$, where μ_{ice} is ice phase fraction, and α_{ice} and α_{liq} are specific cloud microphysical properties. We examined α_{ice} being ice mass fraction or ice particle number fraction at 1-Hz resolution, but also extend the definition to include α_{ice} being ice spatial ratio in a consecutive cloud segment, which is a macrophysical property that has not been investigated before. All three methods follow the same thresholds of < 0.1, 0.1 – 0.9, and >0.9 to separate μ_{ice} into liquid, mixed and ice phases, respectively. As a result, all three methods identify a significant transition from liquid to ice around a similar
315 temperature at -17.5°C. A minor difference among three methods is that mixed-phase cloud frequency between -25°C to 0°C is slightly higher when defined by ice number fraction and ice spatial ratio (0.1 – 0.2) compared with that defined by ice mass fraction (0.05). Such comparison on various phase definition methods indicates that a spatial extent-based cloud phase identification method, such as using number of pixels in remote sensing data by Yip et al. (2021), can produce similar statistical

distributions of liquid and ice phases compared with other methods based on ice mass fraction, e.g., Yang et al. (2021) and

320 D'Alessandro et al. (2019), while the spatial extent-based method produces a slightly higher mixed-phase cloud frequency. Future analysis of cloud phase distributions based on different types of observation techniques and model simulations is recommended to consider this comparison result, especially when evaluating model output against observations using different definitions of mixed-phase clouds.

Differing from previous studies on the coexistence of ice crystals and supercooled liquid water, the method presented in this

325 work allows one to separately examine the cases when ice crystals first start to appear (phase 2) and compare them with cases when ice crystals become more dominant (phase 3). Because of this, aerosol indirect effects on the earlier and later transitions from supercooled liquid water to ice can also be examined separately. Number concentrations of aerosols larger than 500 nm show stronger positive correlations with ice spatial ratio compared with aerosols larger than 100 nm. This indicates that the larger aerosols more likely act as ice nucleating particles to initiate primary ice nucleation. Transition phase 3 shows a weaker

330 positive correlation of ice spatial ratio with aerosols, indicating that the aerosol indirect effects are most prominent when ice crystals first start to appear. Such weaker aerosol indirect effects in phase 3 are possibly due to a competition between the positive correlation of primary ice nucleation with aerosol number concentrations and the negative correlation of secondary ice production with aerosol number concentrations. When pure ice segments (ICR) start to appear, it is possible that secondary ice production plays a more important role and therefore the net aerosol indirect effects become weaker.

335 Thermodynamic and dynamic conditions are examined for each transition phase, especially for two key stages of mixed-phase clouds – the initiation of ice nucleation and the coexistence of liquid and ice after ice being formed. The results show that regions with ice crystals in phase 2 are associated with the highest RH_i values as well as the highest fluctuation of vertical velocity. This result indicates that in-cloud turbulence is likely the main mechanism to produce higher RH_i in order to initiate ice nucleation. Averages of vertical velocity do not show significantly higher values for phase 2, indicating the large-scale

340 ascent plays a less important role for initiating the transition from liquid to ice compared with in-cloud turbulence in the SOCRATES campaign. As for the dynamical conditions supporting the coexistence of liquid and ice, previously, several dynamic mechanisms were proposed in the study of Korolev and Field (2008), highlighting the critical thresholds of vertical motion for sustaining supercooled liquid water. Our analysis shows that both ascent and in-cloud turbulence are more frequently observed when liquid phase becomes more dominant in terms of spatial extent (i.e., low ice spatial ratio). The

345 highest updrafts were observed in transition phase 3 in segments containing both ice and liquid (i.e., MCR), indicating that higher updrafts are needed to sustain supercooled liquid water when they are surrounded by ice crystals. This observation-based method can be used to assess the contribution from different dynamic mechanisms for maintaining different evolution stages of mixed-phase clouds in various field campaigns.

Parameterization of mixed-phase clouds in climate models often relies on a tunable parameter that can modify the mixing

350 volume between ice and liquid (e.g., Tan and Storelvmo, 2016; Zhang et al., 2019). In other words, if ice crystals are mixed uniformly amongst supercooled liquid water within a model grid box, the Bergeron process would become more effective and the transition from liquid to ice would be faster. This study illustrates that the effectiveness of Bergeron process is strongly

affected by the existence of pure ice segments, not only by the ice spatial ratio which reflects how extensive the ice crystals' spatial coverage is (Figure 7). Future model parameterization development is recommended to consider the varying

355 effectiveness of Bergeron process throughout a cloud's lifetime.

Overall, the method proposed in this work provides a unique perspective to assess the evolution of mixed phase clouds, especially the transition from liquid to ice phase. Such transition can be reflected in particle number fraction, mass fraction, and spatial ratio. We note that this is an idealized method with its own caveats. For example, the evolution of mixed-phase clouds may not always follow this direction from phase 1 to 4. In addition, the aircraft observations used here only captures

360 the 1-D structure of a cloud segment, while cloud layers above and below the aircraft flight track may show a different ice spatial ratio on a 2-D or 3-D view. Nevertheless, this method helps to provide a statistical categorization of different evolution phases of mixed-phase clouds solely based on Eulerian-view sampling of aircraft data, which enables more detailed examination on cloud evolution that was not available previously. Future investigation that compares 2-D remote sensing observations with collocated 1-D aircraft sampling is recommended to further assess this method against other types of

365 measurement techniques.

Data availability

Observations from the NSF SOCRATES campaign are accessible at https://data.eol.ucar.edu/.

Author contributions

F. Maciel and M. Diao contributed to the development of the ideas, conducted quality control to aircraft-based observations,
370 and wrote the manuscript. F. Maciel contributed to the subsequent data analysis.

Competing interests

The authors declare that they have no conflict of interest.

Acknowledgments

F. Maciel and M. Diao acknowledge funding from NSF OPP #1744965. F. Maciel also acknowledges support from the San
375 Jose State University Walker Fellowship.

References

Atlas, R., Mohrmann, J., Finlon, J., Lu, J., Hsiao, I., Wood, R., and Diao, M.: The University of Washington Ice–Liquid

Discriminator (UWILD) improves single-particle phase classifications of hydrometeors within Southern Ocean clouds using machine learning, Atmos. Meas. Tech., 14, 7079–7101, https://doi.org/10.5194/amt-14-7079-2021, 2021.

380 Bühl, J., Seifert, P., Engelmann, R., and Ansmann, A.: Impact of vertical air motions on ice formation rate in mixed-phase cloud layers, npj Clim. Atmos. Sci., 2, 36, https://doi.org/10.1038/s41612-019-0092-6, 2019.

D'Alessandro, J. J., Diao, M., Wu, C., Liu, X., Jensen, J. B., and Stephens, B. B.: Cloud phase and relative humidity distributions over the Southern Ocean in austral summer based on in situ observations and CAM5 simulations, J. Clim., 32, https://doi.org/10.1175/JCLI-D-18-0232.1, 2019.

385 D'Alessandro, J. J., McFarquhar, G. M., Wu, W., Stith, J. L., Jensen, J. B., and Rauber, R. M.: Characterizing the Occurrence and Spatial Heterogeneity of Liquid, Ice, and Mixed Phase Low-Level Clouds Over the Southern Ocean Using in Situ Observations Acquired During SOCRATES, J. Geophys. Res. Atmos., 126, e2020JD034482, https://doi.org/https://doi.org/10.1029/2020JD034482, 2021.

DeMott, P. J., Prenni, A. J., Liu, X., Kreidenweis, S. M., Petters, M. D., Twohy, C. H., Richardson, M. S., Eidhammer, T., and
390 Rogers, D. C.: Predicting global atmospheric ice nuclei distributions and their impacts on climate, Proc. Natl. Acad. Sci., 107, 11217–11222, https://doi.org/10.1073/pnas.0910818107, 2010.

Diao, M.: VCSEL 1Hz Water Vapor Data, https://doi.org//10.26023/KFSD-Y8DQ-YC0D, 2021.

Huang, Y., Chubb, T., Baumgardner, D., DeHoog, M., Siems, S. T., and Manton, M. J.: Evidence for secondary ice production in Southern Ocean open cellular convection, Q. J. R. Meteorol. Soc., 143, 1685–1703, https://doi.org/10.1002/qj.3041, 2017.

395 Hyder, P., Edwards, J. M., Allan, R. P., Hewitt, H. T., Bracegirdle, T. J., Gregory, J. M., Wood, R. A., Meijers, A. J. S., Mulcahy, J., Field, P., Furtado, K., Bodas-Salcedo, A., Williams, K. D., Copsey, D., Josey, S. A., Liu, C., Roberts, C. D., Sanchez, C., Ridley, J., Thorpe, L., Hardiman, S. C., Mayer, M., Berry, D. I., and Belcher, S. E.: Critical Southern Ocean climate model biases traced to atmospheric model cloud errors, Nat. Commun., 9, 3625, https://doi.org/10.1038/s41467-018-05634-2, 2018.

400 Jackson, R. C., McFarquhar, G. M., Korolev, A. V, Earle, M. E., Liu, P. S. K., Lawson, R. P., Brooks, S., Wolde, M., Laskin, A., and Freer, M.: The dependence of ice microphysics on aerosol concentration in arctic mixed-phase stratus clouds during ISDAC and M-PACE, J. Geophys. Res. Atmos., 117, https://doi.org/https://doi.org/10.1029/2012JD017668, 2012.

Järvinen, E., McCluskey, C. S., Waitz, F., Schnaiter, M., Bansemer, A., Bardeen, C. G., Gettelman, A., Heymsfield, A., Stith, J. L., Wu, W., D'Alessandro, J. J., McFarquhar, G. M., Diao, M., Finlon, J. A., Hill, T. C. J., Levin, E. J. T., Moore, K. A.,
405 and DeMott, P. J.: Evidence for Secondary Ice Production in Southern Ocean Maritime Boundary Layer Clouds, J. Geophys. Res. Atmos., 127, https://doi.org/10.1029/2021JD036411, 2022.

Korolev, A., Isaac, G. A., Cober, S. G., Strapp, J. W., and Hallett, J.: Microphysical characterization of mixed-phase clouds, Q. J. R. Meteorol. Soc., 129, 39–65, https://doi.org/https://doi.org/10.1256/qj.01.204, 2003.

Korolev, A. V. and Field, P. R.: The Effect of Dynamics on Mixed-Phase Clouds: Theoretical Considerations, J. Atmos. Sci.,
410 65, 66–86, https://doi.org/10.1175/2007JAS2355.1, 2008.

Korolev, A. V., Strapp, J. W., Isaac, G. A., and Nevzorov, A. N.: The Nevzorov Airborne Hot-Wire LWC–TWC Probe:

Principle of Operation and Performance Characteristics, J. Atmos. Ocean. Technol., 15, 1495–1510, https://doi.org/10.1175/1520-0426(1998)015<1495:TNAHWL>2.0.CO;2, 1998.

Korolev, A., McFarquhar, G., Field, P. R., Franklin, C., Lawson, P., Wang, Z., Williams, E., Abel, S. J., Axisa, D., Borrmann, S., Crosier, J., Fugal, J., Krämer, M., Lohmann, U., Schlenczek, O., Schnaiter, M., and Wendisch, M.: Mixed-Phase Clouds: Progress and Challenges, Meteorol. Monogr., 58, 5.1-5.50, https://doi.org/10.1175/AMSMONOGRAPHS-D-17-0001.1, 2017.

Matus, A. V and L'Ecuyer, T. S.: The role of cloud phase in Earth's radiation budget, J. Geophys. Res. Atmos., 122, 2559–2578, https://doi.org/https://doi.org/10.1002/2016JD025951, 2017.

McCluskey, C. S., Hill, T. C. J., Humphries, R. S., Rauker, A. M., Moreau, S., Strutton, P. G., Chambers, S. D., Williams, A. G., McRobert, I., Ward, J., Keywood, M. D., Harnwell, J., Ponsonby, W., Loh, Z. M., Krummel, P. B., Protat, A., Kreidenweis, S. M., and DeMott, P. J.: Observations of Ice Nucleating Particles Over Southern Ocean Waters, Geophys. Res. Lett., 45, 11,989-11,997, https://doi.org/10.1029/2018GL079981, 2018.

McFarquhar, G. M., Bretherton, C. S., Marchand, R., Protat, A., DeMott, P. J., Alexander, S. P., Roberts, G. C., Twohy, C. H., Toohey, D., Siems, S., Huang, Y., Wood, R., Rauber, R. M., Lasher-Trapp, S., Jensen, J., Stith, J. L., Mace, J., Um, J., Järvinen, E., Schnaiter, M., Gettelman, A., Sanchez, K. J., McCluskey, C. S., Russell, L. M., McCoy, I. L., Atlas, R. L., Bardeen, C. G., Moore, K. A., Hill, T. C. J., Humphries, R. S., Keywood, M. D., Ristovski, Z., Cravigan, L., Schofield, R., Fairall, C., Mallet, M. D., Kreidenweis, S. M., Rainwater, B., D'Alessandro, J., Wang, Y., Wu, W., Saliba, G., Levin, E. J. T., Ding, S., Lang, F., Truong, S. C. H., Wolff, C., Haggerty, J., Harvey, M. J., Klekociuk, A. R., and McDonald, A.: Observations of Clouds, Aerosols, Precipitation, and Surface Radiation over the Southern Ocean: An Overview of CAPRICORN, MARCUS, MICRE, and SOCRATES, Bull. Am. Meteorol. Soc., 102, E894–E928, https://doi.org/10.1175/BAMS-D-20-0132.1, 2021.

Mohrmann, J., et al. 2021. University of Washington Ice-Liquid Discriminator single particle phase classifications and 1 Hz particle size distributions/heterogeneity estimate. Version 1.0. UCAR/NCAR - Earth Observing Laboratory. https://doi.org/10.26023/PA5W-4DRX-W50A. Accessed 21 Aug 2022.

Morrison, H., de Boer, G., Feingold, G., Harrington, J., Shupe, M. D., and Sulia, K.: Resilience of persistent Arctic mixed-phase clouds, Nat. Geosci., 5, 11–17, https://doi.org/10.1038/ngeo1332, 2012.

Murphy, D. M. and Koop, T.: Review of the vapour pressures of ice and supercooled water for atmospheric applications, Q. J. R. Meteorol. Soc., 131, 1539–1565, https://doi.org/10.1256/qj.04.94, 2005.

Norgren, M. S., de Boer, G., and Shupe, M. D.: Observed aerosol suppression of cloud ice in low-level Arctic mixed-phase clouds, Atmos. Chem. Phys., 18, 13345–13361, https://doi.org/10.5194/acp-18-13345-2018, 2018.

Qiu, S., Xi, B., and Dong, X.: Influence of Wind Direction on Thermodynamic Properties and Arctic Mixed-Phase Clouds in Autumn at Utqiaġvik, Alaska, J. Geophys. Res. Atmos., 123, 9589–9603, https://doi.org/https://doi.org/10.1029/2018JD028631, 2018.

Shupe, M. D., Kollias, P., Persson, P. O. G., and McFarquhar, G. M.: Vertical Motions in Arctic Mixed-Phase Stratiform Clouds, J. Atmos. Sci., 65, 1304–1322, https://doi.org/10.1175/2007JAS2479.1, 2008.

Storelvmo, T.: Aerosol Effects on Climate via Mixed-Phase and Ice Clouds, Annu. Rev. Earth Planet. Sci., 45, 199–222,

https://doi.org/10.1146/annurev-earth-060115-012240, 2017.

Tan, I., Storelvmo, T., and Zelinka, M. D.: Observational constraints on mixed-phase clouds imply higher climate sensitivity, Science (80-.)., 352, 224–227, https://doi.org/10.1126/science.aad5300, 2016.

Tan, I. and Storelvmo, T.: Sensitivity Study on the Influence of Cloud Microphysical Parameters on Mixed-Phase Cloud
450 Thermodynamic Phase Partitioning in CAM5, J. Atmos. Sci., 73, 709–728, https://doi.org/10.1175/JAS-D-15-0152.1, 2016.

Wang, Y., McFarquhar, G. M., Rauber, R. M., Zhao, C., Wu, W., Finlon, J. A., Stechman, D. M., Stith, J., Jensen, J. B., Schnaiter, M., Järvinen, E., Waitz, F., Vivekanandan, J., Dixon, M., Rainwater, B., and Toohey, D. W.: Microphysical Properties of Generating Cells Over the Southern Ocean: Results From SOCRATES, J. Geophys. Res. Atmos., 125, e2019JD032237, https://doi.org/https://doi.org/10.1029/2019JD032237, 2020.

455 Yang, C. A., Diao, M., Gettelman, A., Zhang, K., Sun, J., McFarquhar, G., and Wu, W.: Ice and Supercooled Liquid Water Distributions Over the Southern Ocean Based on In Situ Observations and Climate Model Simulations, J. Geophys. Res. Atmos., 126, https://doi.org/10.1029/2021JD036045, 2021.

Yip, J., Diao, M., Silber, I., and Gettelman, A.: Evaluation of the CAM6 Climate Model Using Cloud Observations at McMurdo Station, Antarctica, J. Geophys. Res. - Atmos., 126, e2021JD034653, https://doi.org/10.1029/2021JD034653, 2021.

460 Zaremba, T. J., Rauber, R. M., McFarquhar, G. M., Hayman, M., Finlon, J. A., and Stechman, D. M.: Phase Characterization of Cold Sector Southern Ocean Cloud Tops: Results From SOCRATES, J. Geophys. Res. Atmos., 125, e2020JD033673, https://doi.org/https://doi.org/10.1029/2020JD033673, 2020.

Zhang, M., Liu, X., Diao, M., D'Alessandro, J. J., Wang, Y., Wu, C., Zhang, D., Wang, Z., and Xie, S.: Impacts of Representing Heterogeneous Distribution of Cloud Liquid and Ice on Phase Partitioning of Arctic Mixed-Phase Clouds with NCAR CAM5,
465 J. Geophys. Res. Atmos., 124, 13071–13090, https://doi.org/10.1029/2019JD030502, 2019.

Zhao, X. and Liu, X.: Global Importance of Secondary Ice Production, Geophys. Res. Lett., 48, https://doi.org/10.1029/2021GL092581, 2021.

Table 1. Definitions of four transition phases of mixed-phase clouds, alongside their required spatial ratios.

Phase	Description	Liquid Spatial Ratio	Ice Spatial Ratio	Mixed Spatial Ratio
		M1 = length of LCR / total segment length	M2 = length of ICR / total segment length	M3 = length of MCR / total segment length
1	Only LCR	M1 = 1	M2 = 0	M3 = 0
2	MCR appears	0 < M1 < 0	M2 = 0	0 < M3 ≤ 1
3	Pure ICR must appear	0 ≤ M1 < 1	0 < M2 < 1	0 ≤ M3 < 1
4	Only ICR	M1 = 0	M2 = 1	M3 = 0

470
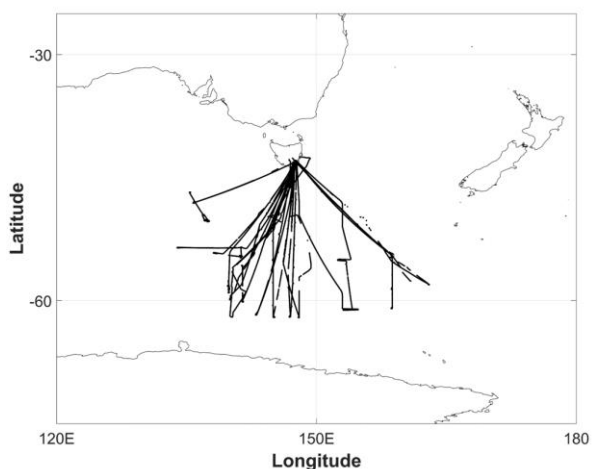
Figure 1. Map of the flight tracks for SOCRATES for only temperatures between 0°C and -40°C.
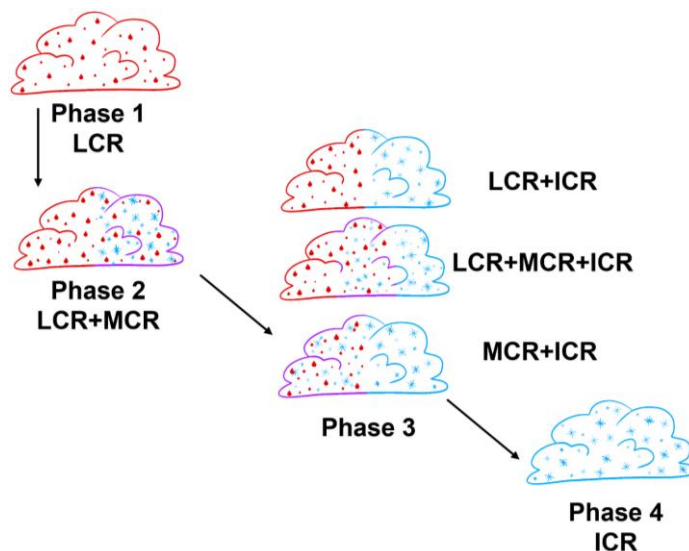
Figure 2. An idealized diagram of the four transition phases for mixed-phase cloud evolution. Red, blue and purple shading indicates liquid cloud region (LCR), ice cloud region (ICR) and mixed cloud region (MCR), respectively.
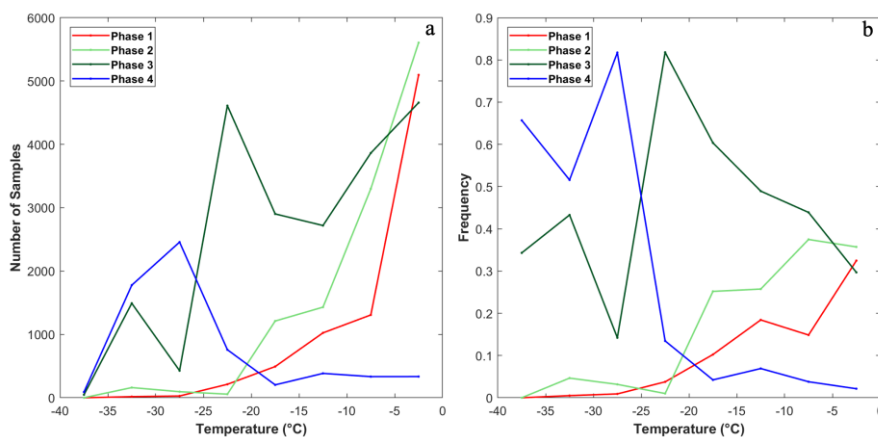
Figure 3. Distributions of four transition phases at various temperatures. (a) Number of samples and (b) probability of each phase. The probability is normalized by the number of samples of all phases in each 5-degree temperature bin.
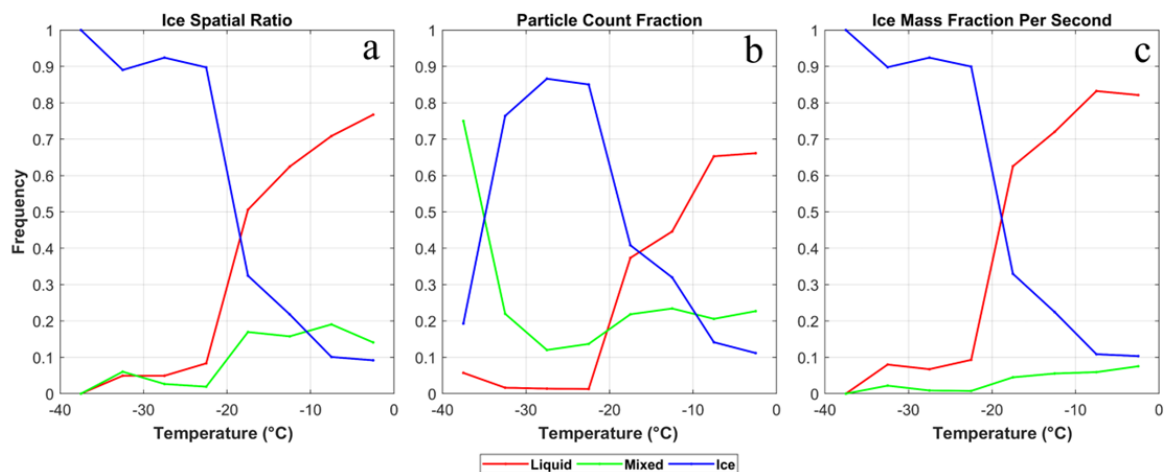
Figure 4. Cloud phase occurrence frequencies at various temperatures. Cloud phase identification methods based on (a) ice spatial ratio for an entire in-cloud segment, (b) ice particle number fraction per second, and (c) ice mass fraction per second.
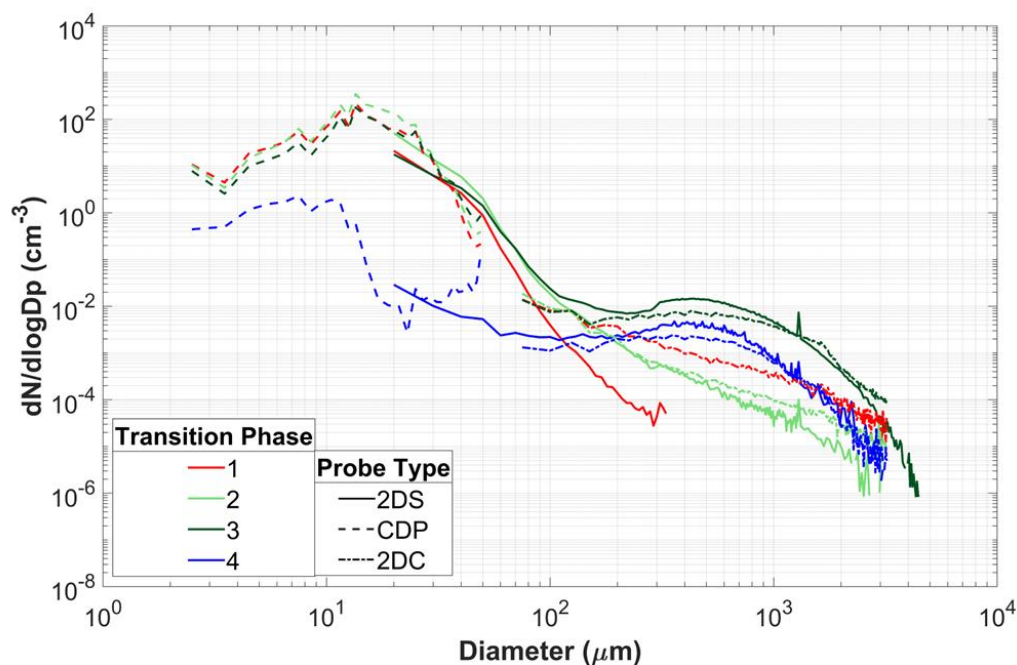
Figure 5. Particle size distribution of the four transition phases for mixed-phase clouds separated by probe type.
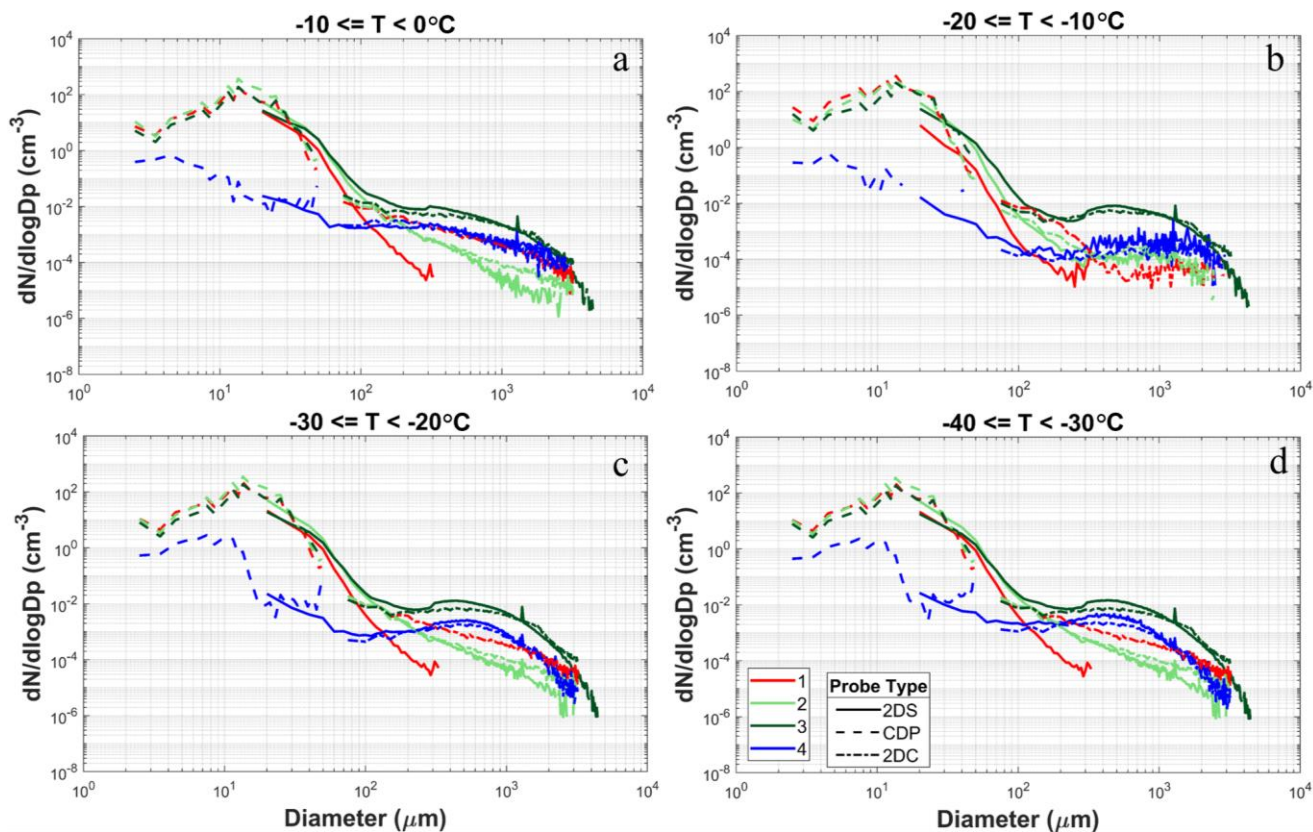
490

Figure 6. Similar to Figure 5, but separated into four temperature ranges.
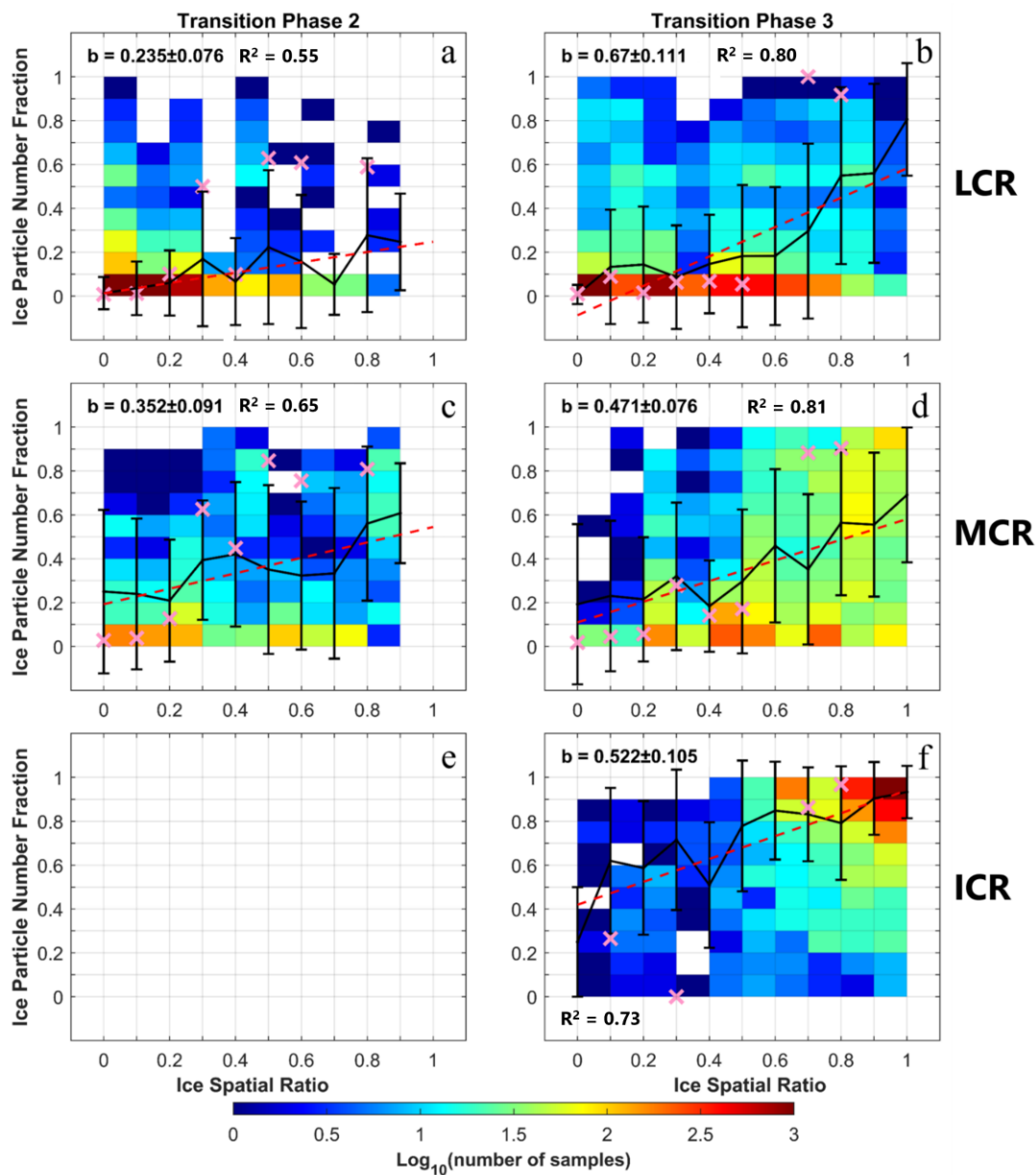
Figure 7. Relationship between ice particle number fraction and ice spatial ratio, separated by the transition phases (phase 2 in column 1 and phase 3 in column 2), and by various cloud segments – (a, b) LCR, (c, d) MCR and (e, f) ICR. Average values for each ice spatial ratio bin are shown black solid line, with vertical bars representing standard deviations. Linear fit is shown in red dashed line. Average values of generating cells (time series obtained from Wang et al. (2020)) are in purple. The slope value b, and its associated error are also shown along with the ordinary R-squared value.
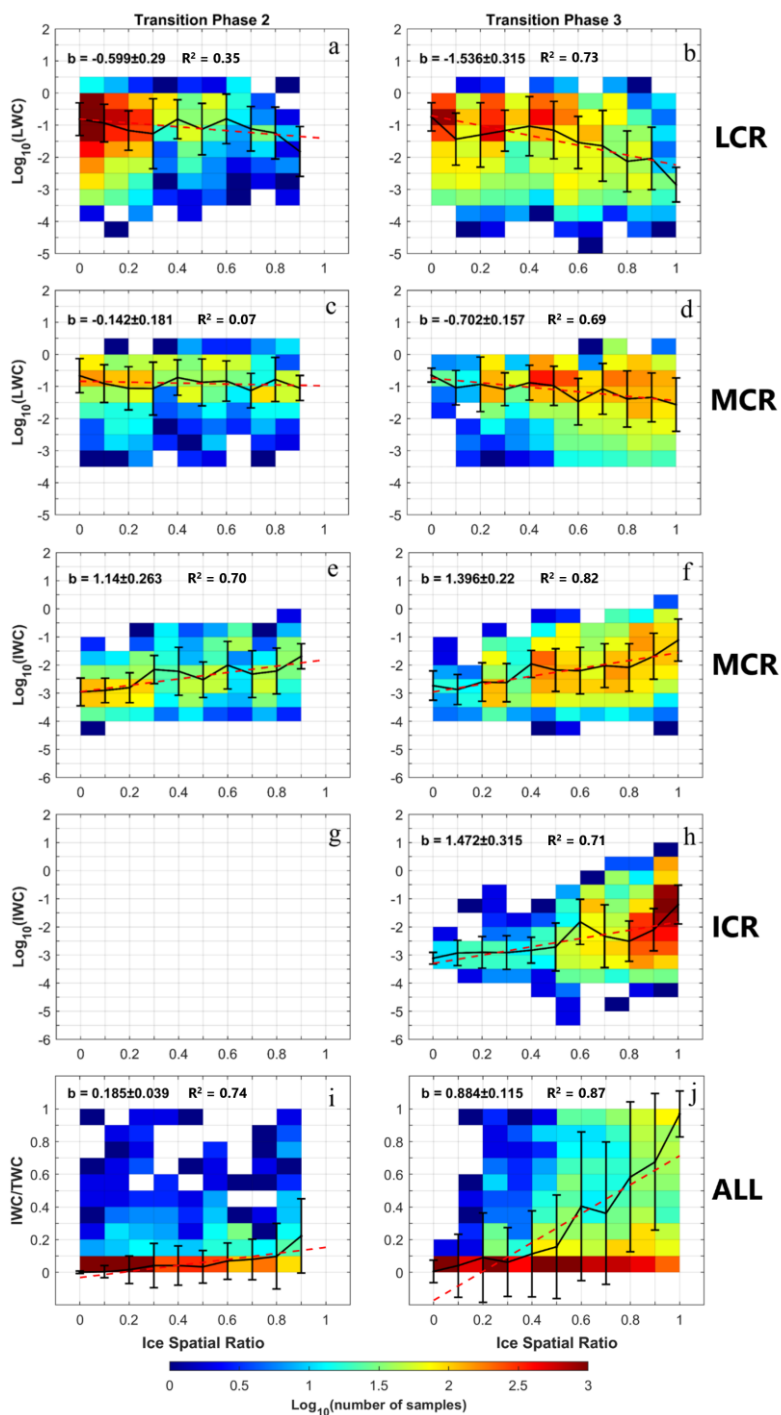
Figure 8. Similar to Figure 7, but showing (a-d) LWC, (e-h) IWC, and (i and j) ice mass fraction in relation to ice spatial ratio, separated by the transition phases and cloud regions.
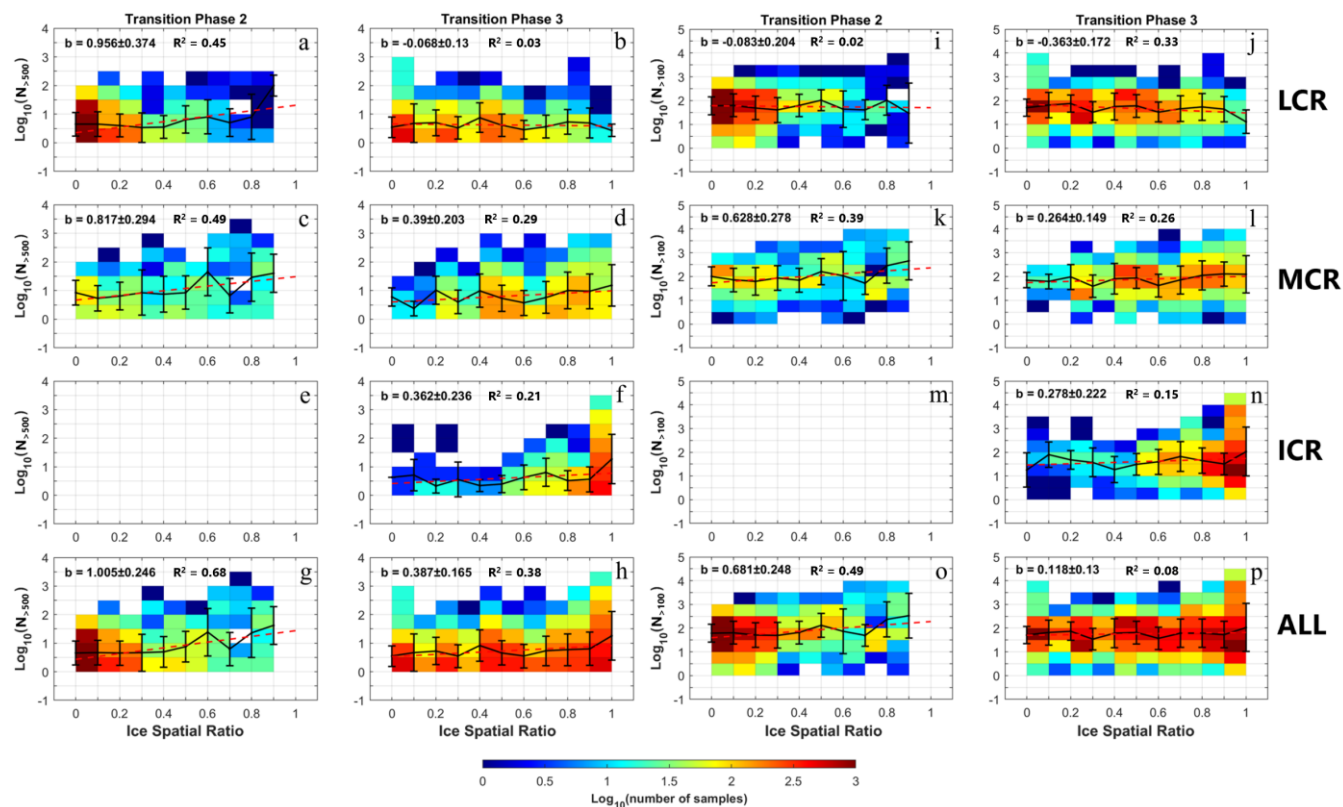
Figure 9. Similar to Figure 7, but showing logarithmic scale (a-h) $N_{>500}$ and (i-p) $N_{>100}$ in relation to ice spatial ratio,
separated by the transition phases and cloud regions. The last row represents all cloud regions in a specific transition phase.
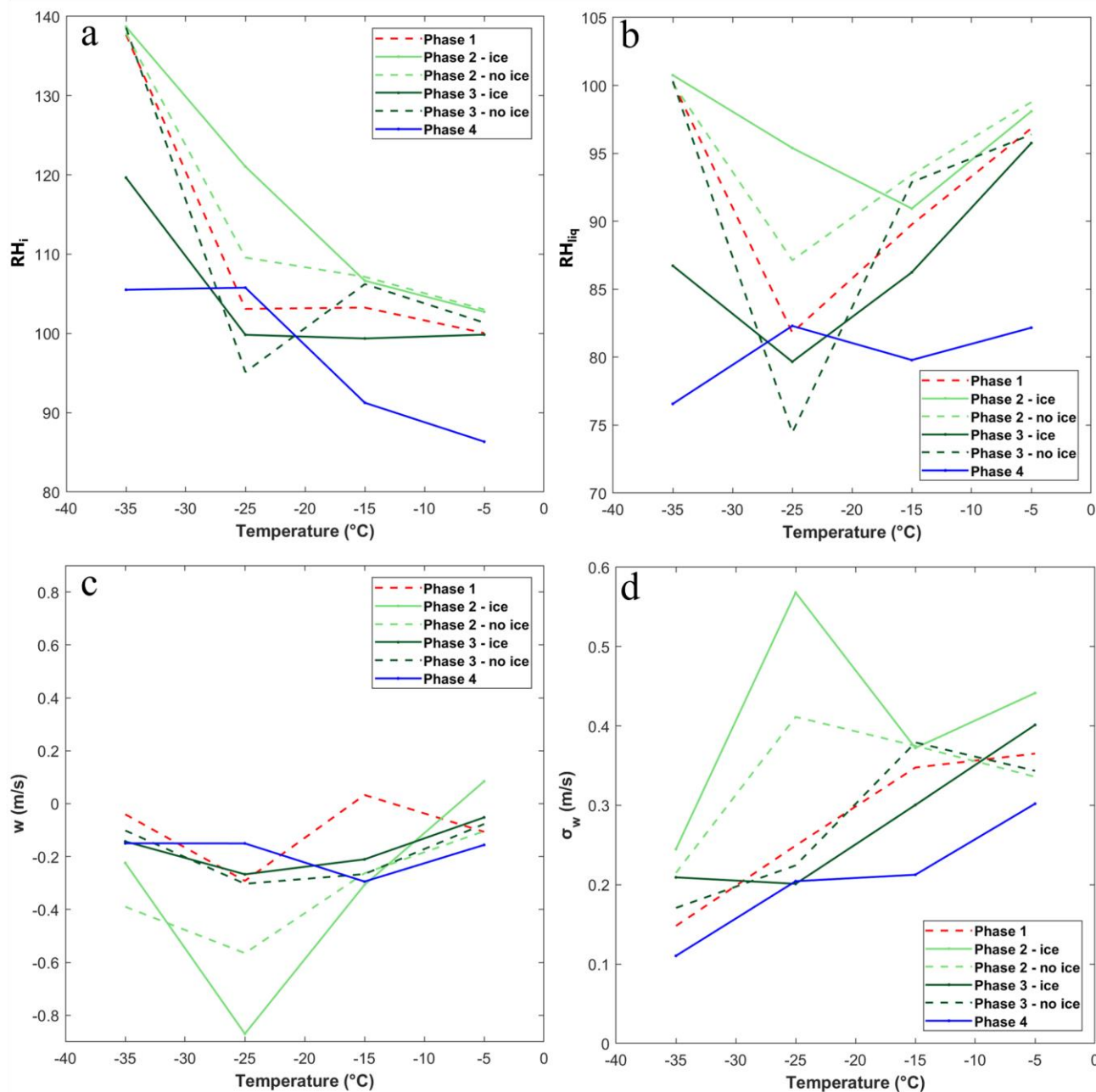
Figure 10. Distributions of (a) RH_i, (b) RH_{liq}, (c) vertical velocity (w) and (d) standard deviation of vertical velocity (σ_w) for various transition phases at different temperatures.
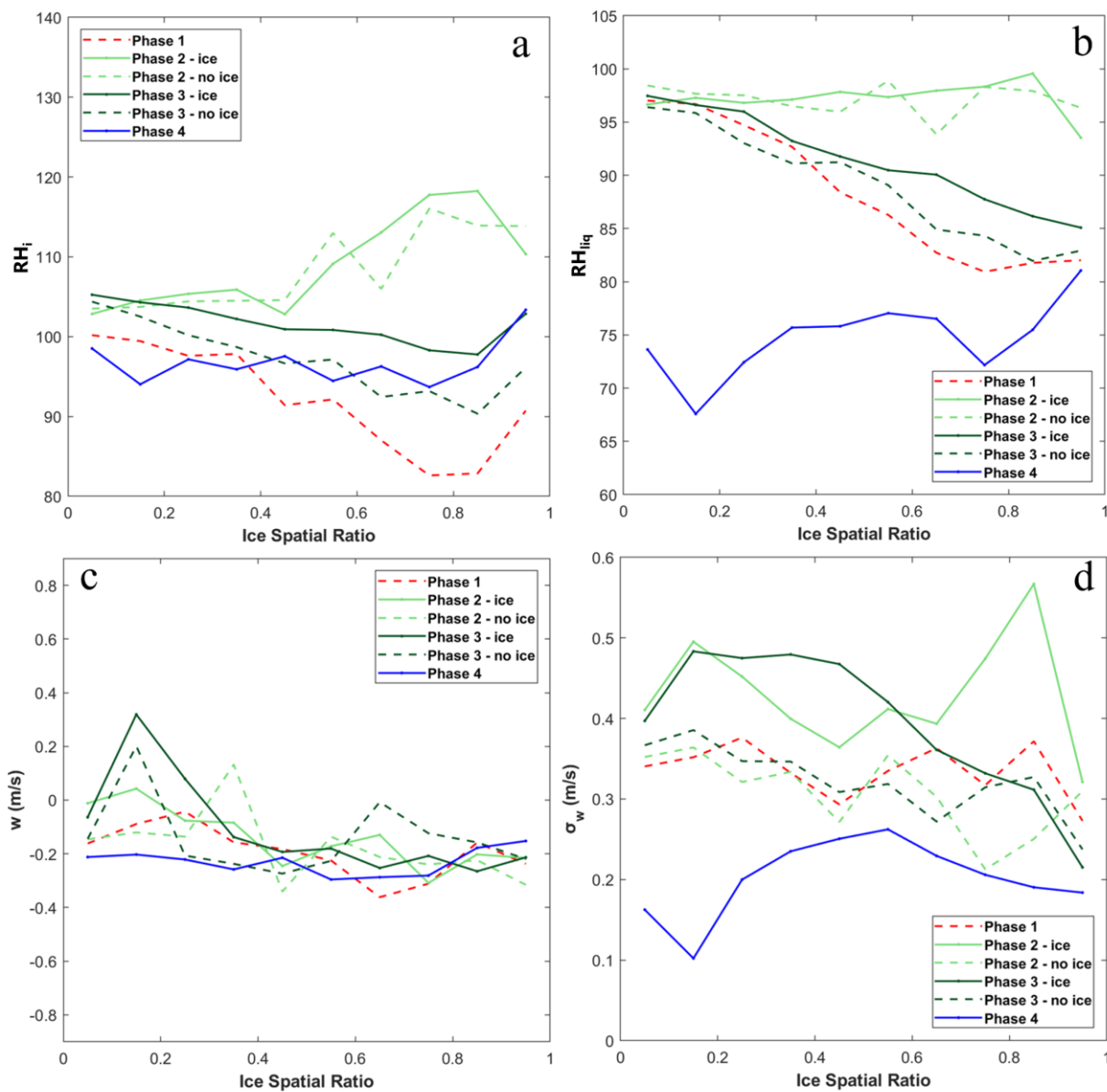
Figure 11. Similar to Figure 10, but in relation to various ice spatial ratios.

510